Jacobi-like bar mode instability of relativistic rotating bodies

Dorota Gondek-Rosińska* and Eric Gourgoulhon†
Laboratoire de l'Univers et de ses Théories, FRE 2462 du C.N.R.S.,
Observatoire de Paris, F-92195 Meudon Cedex, France
(Dated: 23 May 2002)

We perform some numerical study of the secular triaxial instability of rigidly rotating homogeneous fluid bodies in general relativity. In the Newtonian limit, this instability arises at the bifurcation point between the Maclaurin and Jacobi sequences. It can be driven in astrophysical systems by viscous dissipation. We locate the onset of instability along several constant baryon mass sequences of uniformly rotating axisymmetric bodies for compaction parameter $M/R = 0 - 0.275$. We find that general relativity weakens the Jacobi like bar mode instability, but the stabilizing effect is not very strong. According to our analysis the critical value of the ratio of the kinetic energy to the absolute value of the gravitational potential energy $(T/|W|)_{\rm crit}$ for compaction parameter as high as 0.275 is only 30% higher than the Newtonian value. The critical value of the eccentricity depends very weakly on the degree of relativity and for $M/R = 0.275$ is only 2% larger than the Newtonian value at the onset for the secular bar mode instability. We compare our numerical results with recent analytical investigations based on the post-Newtonian expansion.

PACS numbers: 04.40.Dg, 04.30.Db, 04.25.Dm, 97.10.Kc, 97.60.Jd

I. INTRODUCTION

A. The Maclaurin-Jacobi bifurcation point

In Newtonian theory a self-gravitating incompressible fluid body rotating at a moderate velocity around a fixed axis with respect to some inertial frame takes the shape of a Maclaurin ellipsoid, which is axisymmetric with respect to the rotation axis. For a higher rotation rate, namely when the ratio of kinetic to gravitational potential energy $T/|W|$ is larger than 0.1375, another figure of equilibrium exists: that of a Jacobi ellipsoid, which is triaxial and rotates around its smallest axis [1]. Actually the Jacobi ellipsoid is a preferred figure of equilibrium, since at fixed mass and angular momentum, it has a lower total energy $E = T + W$ than a Maclaurin ellipsoid, due to its greater moment of inertia I with respect to the rotation axis. Indeed, at fixed angular momentum J, the kinetic energy $T = J^2/(2I)$ is a decreasing function of I, and for large values of J, this decrease overcomes the effect of the gravitational potential energy W, which increases with I. Therefore, provided some mechanism acts for dissipating energy while preserving angular momentum (for instance viscosity), a Maclaurin ellipsoid with $T/|W| > 0.1375$ will break its axial symmetry and migrate toward a Jacobi ellipsoid [2, 3, 4]. This is the secular "bar mode" instability of rigidly rapidly rotating bodies. The qualifier *secular* reflects the necessity of some dissipative mechanism to lower the energy, the instability growth rate being controlled by the dissipation time scale[1]. As shown by Christodoulou et al. [4], the Jacobi-like bar mode instability appears only if the fluid circulation is not conserved. If on the contrary, the circulation is conserved (as in inviscid fluids submitted only to potential forces), but not the angular momentum, it is the Dedekind-like instability which develops instead. The famous Chandrasekhar-Friedman-Schutz (CFS) instability (see [5] for a review) belongs to this category.

The Jacobi-like bar mode instability, applied to neutron stars, is particularly relevant to gravitational wave astrophysics. Indeed a Jacobi ellipsoid has a time varying mass quadrupole moment with respect to any inertial frame, and therefore emits gravitational radiation, unlike a Maclaurin spheroid. For a rapidly rotating neutron star, the typical frequency of gravitational waves (twice the rotation frequency) falls in the bandwidth of the interferometric detectors LIGO and VIRGO currently under construction.

Neutron stars being highly relativistic objects, the classical critical value $T/|W| = 0.1375$, established for incompressible Newtonian bodies, cannot a priori be applied to them. The aim of the present article is thus to investigate

*Dorota.Gondek@obspm.fr; also at Nicolaus Copernicus Astronomical Center, Bartycka 18, 00-716 Warszawa, Poland
†Eric.Gourgoulhon@obspm.fr
[1] For $T/|W| \geq 0.2738$, the Maclaurin spheroids are subject to another instability, which is on the contrary *dynamical*, i.e. it develops independently of any dissipative mechanism and on a dynamical time scale (one rotation period).

the effect of general relativity on the secular bar mode instability of homogeneous incompressible bodies. We do not discuss compressible fluids here. It has been shown that compressibility has little effect on the triaxial instability [6].

B. Previous studies in the relativistic regime

Chandrasekhar [7, 8] has examined the first order post-Newtonian (PN) corrections to the Maclaurin and Jacobi ellipsoids, by means of the tensor virial formalism. This work has been revisited recently by Taniguchi [9]. However, these authors have not computed the location of the Maclaurin-Jacobi bifurcation point at the 1-PN level. This has been done only recently by Shapiro & Zane [10] and Di Girolamo & Vietri [11].

On the numerical side, Bonazzola, Frieben & Gourgoulhon [12, 13] have investigated the secular bar mode instability of rigidly rotating compressible stars in general relativity. In the Newtonian limit, they recover the classical result of James [14] (see also [15]), namely that, for a polytropic equation of state, the adiabatic index must be larger than $\gamma_{\rm crit} = 2.238$ for the bifurcation point to occur before the mass shedding limit (Keplerian frequency). In the relativistic regime, they have shown that general relativistic effects stabilize rotating stars against the viscosity driven triaxial instability. In particular, they have found that $\gamma_{\rm crit}$ is an increasing function of the stellar compactness, reaching $\gamma_{\rm crit} \sim 2.8$ for a typical neutron star compaction parameter. This stabilizing tendency of general relativity has been confirmed by the PN study of Shapiro & Zane [10] and Di Girolamo & Vietri [11] mentioned above. Note that this behavior contrasts with the CFS instability, which is strengthened by general relativity [16, 17].

C. The present work

In this paper, we improve the numerical technique over that used by Bonazzola et al. [12, 13] by introducing surface fitted coordinates, which enable us to treat the density discontinuity at the surface of incompressible bodies. Indeed the technique used in Refs. [12, 13] did not permit to compute any incompressible model. In particular, it was not possible to compare the numerical results in the Newtonian limit with the classical Maclaurin-Jacobi bifurcation point. We shall perform such a comparison here. The very good agreement obtained (relative discrepancy $\sim 10^{-6}$) provides very strong support for the method we use for locating the bifurcation point and which is essentially the same as that presented in Ref. [13].

The plan of the paper is as follows. The analytical formulation of the problem, including the approximations we introduce, is presented in Sec. II. Section III then describes the numerical technique we employ, as well as the various tests passed by the numerical code. The numerical results are presented in Sec. IV, as well as a detailed comparison with the PN studies [10] and [11]. Finally, Sec. V provides some summary of our work.

II. BASIC ASSUMPTIONS AND EQUATIONS TO BE SOLVED

A. Helical symmetry

Let us consider a rotating star that is steadily increasing its rotation rate, e.g. by accretion in a binary system. Before the triaxial instability sets in, the spacetime generated by the rotating star can be considered as *stationary* and *axisymmetric*, which means that there exist two Killing vector fields, $\mathbf{k}$ and $\mathbf{m}$, such that $\mathbf{k}$ is timelike (at least far from the star) and $\mathbf{m}$ is spacelike and its orbits are closed curves.

When the axisymmetry of the star is broken, the stationarity of spacetime is also broken. In Newtonian theory, there is no inertial frame in which a rotating triaxial object appears stationary, i.e. does not depend upon the time. It can be stationary only in a corotating frame, which is not inertial, so that the stationarity is broken in this sense. The stationarity in the corotating frame can be expressed geometrically by stating that the Newtonian spacetime possesses a one-parameter symmetry group, whose integral curves are helices. A generator of this symmetry group thus has the form

$$\boldsymbol{\ell} = \frac{\partial}{\partial t} + \Omega \, \frac{\partial}{\partial \varphi} \ , \tag{1}$$

where t and φ are respectively the time and azimuthal coordinates associated with an inertial observer, and Ω is the angular velocity with respect to the inertial frame.

In general relativity, a rotating triaxial system cannot be stationary, even in the corotating frame, as it radiates away gravitational waves and therefore loses energy and angular momentum. However, at the very point of the

symmetry breaking, no gravitational wave has yet been emitted. For sufficiently small deviations from axisymmetry, we may neglect the gravitational radiation. Therefore we shall assume that the spacetime has a helical symmetry, as in the Newtonian case. The (suitably normalized) associated symmetry generator $\boldsymbol{\ell}$ is then a Killing vector, which can be written in the form (1) in weak-field regions (spacelike infinity). Note that spacetimes with helical symmetry have been also used for describing binary systems with circular orbits [18, 19, 20, 21, 22].

B. Rigid rotation

We model the stellar matter by a perfect fluid, for which the stress-energy tensor takes the form $\mathbf{T} = (e+p)\mathbf{u}\otimes\mathbf{u} + p\,\mathbf{g}$, where $\mathbf{u}$ is the fluid 4-velocity, e the fluid proper energy density, p the fluid pressure and $\mathbf{g}$ the spacetime metric tensor.

A rigid motion is defined in relativity by the vanishing of the expansion tensor $\theta_{\alpha\beta} := (g_\alpha{}^\mu + u_\alpha u^\mu)(g_\beta{}^\nu + u_\beta u^\nu)\nabla_{(\nu} u_{\mu)}$ of the 4-velocity $\mathbf{u}$. In presence of the Killing vector $\boldsymbol{\ell}$, this can be realized by requiring the colinearity of $\mathbf{u}$ and $\boldsymbol{\ell}$ (supposing that the fluid occupies only the region where $\boldsymbol{\ell}$ is timelike) :

$$\mathbf{u} = \lambda\, \boldsymbol{\ell}\ , \tag{2}$$

where λ is a scalar field related to the norm of $\boldsymbol{\ell}$ by the normalization of the 4-velocity $\lambda = (-\boldsymbol{\ell}\cdot\boldsymbol{\ell})^{-1/2}$.

For a perfect fluid at zero temperature, the momentum-energy conservation equation $\nabla\cdot\mathbf{T} = 0$ can be recast as [23, 24]

$$\mathbf{u}\cdot(\nabla\wedge\boldsymbol{\pi}) = 0 \tag{3}$$

$$\nabla\cdot(n\mathbf{u}) = 0\ , \tag{4}$$

where n is the proper baryon number density and $\boldsymbol{\pi}$ is the momentum 1-form $\boldsymbol{\pi} := h\mathbf{u}$, h being the fluid specific enthalpy: $h := (e+p)/(m_{\rm B} n)$, where $m_{\rm B}$ is some mean baryon mass. In Eq. (3), $\nabla\wedge\boldsymbol{\pi}$ denotes the exterior derivative of $\boldsymbol{\pi}$, the so-called *vorticity 2-form* [23]. For the rigid motion we are considering, the baryon number conservation equation (4) is automatically satisfied, thanks to the colinearity of $\mathbf{u}$ with the symmetry generator $\boldsymbol{\ell}$. Moreover, the equation of motion (3) can be reduced to a first integral. Indeed Cartan's identity applied to the Lie derivative of the 1-form $\boldsymbol{\pi}$ along the vector field $\boldsymbol{\ell}$ leads to

$$\pounds_{\boldsymbol{\ell}}\boldsymbol{\pi} = \boldsymbol{\ell}\cdot(\nabla\wedge\boldsymbol{\pi}) + \nabla(\boldsymbol{\ell}\cdot\boldsymbol{\pi}) = 0\ , \tag{5}$$

where the second equality holds thanks to the helical symmetry: $\pounds_{\boldsymbol{\ell}}\boldsymbol{\pi} = 0$. Inserting relation (2) into the equation of fluid motion (3) shows that the first term in Eq. (5) vanishes identically, so that one gets the first integral of motion [24]

$$\boldsymbol{\ell}\cdot\boldsymbol{\pi} = -\lambda^{-1} h = \text{const.} \tag{6}$$

In the axisymmetric and stationary case, where $\boldsymbol{\ell}$ is a linear combination of the two Killing vectors [Eq. (14) below], one recovers the classical expression [25].

The first integral (6) can be re-expressed in terms of the 3+1 formalism of general relativity. Let us introduce the spacetime foliation by the $t =$ const hypersurfaces Σ_t and the associated future-directed unit vector field $\mathbf{n}$ everywhere normal to Σ_t. $\mathbf{n}$ is the 4-velocity of the so-called *Eulerian observer* (also called *ZAMO* or *locally non-rotating observer*). We have the following orthogonal split of the fluid 4-velocity:

$$\mathbf{u} = \Gamma(\mathbf{n} + \mathbf{U}) \qquad \text{with} \quad \mathbf{n}\cdot\mathbf{U} = 0\ , \tag{7}$$

with the Lorentz factor

$$\Gamma = -\mathbf{n}\cdot\mathbf{u} = (1 - \mathbf{U}\cdot\mathbf{U})^{-1/2}\ . \tag{8}$$

The spacelike vector $\mathbf{U}$ is the fluid 3-velocity as measured by the Eulerian observer and the second equality in the above equation results from the normalization of the 4-velocity $\mathbf{u}$. Similarly, we have an orthogonal split of the helical Killing vector:

$$\boldsymbol{\ell} = N\mathbf{n} + \mathbf{B} \qquad \text{with} \quad \mathbf{n}\cdot\mathbf{B} = 0\ , \tag{9}$$

where N is the lapse function, governing the proper time evolution between two neighboring hypersurfaces Σ_t. From relation (2) and the two orthogonal decompositions (7) and (9), we get $\lambda = \Gamma/N$, so that the (logarithm of the) first integral (6) can be written

$$H + \nu - \ln\Gamma = \text{const.} \tag{10}$$

with

$$H := \ln h \qquad \text{and} \qquad \nu := \ln N \ . \tag{11}$$

In the non-relativistic limit, H tends toward the classical specific enthalpy (excluding the rest-mass energy) of the fluid, whereas ν tends toward the Newtonian gravitational potential. Therefore, in the Newtonian limit, where $\ln\Gamma \to \mathbf{U}^2/2$ and $\mathbf{U} \to \mathbf{\Omega} \times \mathbf{r}$, Eq. (10) reduces to the classical first integral of motion

$$H + \nu - \frac{1}{2}(\mathbf{\Omega} \times \mathbf{r})^2 = \text{const.} \tag{12}$$

C. Einstein equations

When the rigidly rotating star is still stationary and axisymmetric, it is well known that a coordinate system $x^\mu = (t, r, \theta, \varphi)$ can be chosen so that the metric takes the Papapetrou form (see e.g. [26] and references therein)

$$g_{\mu\nu}\, dx^\mu dx^\nu = -N^2\, \mathrm{d}t^2 + B^2 r^2 \sin^2\theta (\mathrm{d}\varphi - N^\varphi \mathrm{d}t)^2 + A^2(\mathrm{d}r^2 + r^2 \mathrm{d}\theta^2) \ , \tag{13}$$

where N, N^φ, A and B are four functions of (r, θ). The coordinate vectors $\partial/\partial t$ and $\partial/\partial\varphi$ are then the two Killing vectors $\mathbf{k}$ and $\mathbf{m}$ mentioned in Sec. II A. The helical Killing vector $\boldsymbol{\ell}$ is expressible as

$$\boldsymbol{\ell} = \mathbf{k} + \Omega \mathbf{m} \ . \tag{14}$$

With the form (13), the Einstein equations reduce to a set of four coupled elliptic equations (see e.g. [27] for the precise form).

When the triaxial instability sets in, we shall consider that the metric is a perturbation of (13), which we write as [13]

$$g_{\mu\nu}\, dx^\mu dx^\nu = -N^2\, \mathrm{d}t^2 + B^2 r^2 \sin^2\theta (\mathrm{d}\varphi - N^\varphi \mathrm{d}t)^2 + A^2(\mathrm{d}r - N^r \mathrm{d}t)^2 + r^2 A^2 (\mathrm{d}\theta - N^\theta \mathrm{d}t)^2 \ , \tag{15}$$

where N, N^r, N^θ, N^φ, A and B are six functions of (r, θ, φ'), with

$$\varphi' := \varphi - \Omega t \ . \tag{16}$$

Note that $\partial/\partial t$ and $\partial/\partial\varphi$ are no longer Killing vectors, only $\boldsymbol{\ell}$ remains Killing. The coordinate system $x^{\mu'} = (t, r, \theta, \varphi')$ is adapted to the Killing vector $\boldsymbol{\ell}$ and t is an ignorable coordinate in this system. We call $x^{\mu'}$ the *corotating* coordinate system, and x^μ the *nonrotating* one. N is the lapse function already introduced in Eq. (9). $N^i = (N^r, N^\theta, N^\varphi)$ is (minus[2]) the *shift vector* of the nonrotating coordinate system.

In the triaxial case, there is no equivalent of the Papapetrou theorem [28, 29, 30] which, in absence of convective motions (in the meridional planes), allows one to set to zero all the off-diagonal components of the metric tensor of axisymmetric and stationary spacetimes, except for $g_{t\varphi}$. So, in principle, all the metric components should be non-vanishing in Eq. (15). However, we retained only g_{tr} and $g_{t\theta}$ as the extra non zero components with respect to the axisymmetric case. We did so as an approximation in order to simplify the writing of Einstein equations. This approximation can be justified by the following remarks: (i) the metric element (15) is exact in the stationary axisymmetric case, (ii) it encompasses the first order PN metric. This means that the neglected terms are of second order PN and moreover vanish for stationary axisymmetric rotating stars. We consider these terms to be negligible in our study of the verge of the non-axisymmetric instability.

---

[2] In numerical relativity, the current convention is to call *shift vector* the 3-vector $\beta^i = -N^i$.

The Einstein equation leads to the following set of partial differential equations:

$$\underline{\Delta}\,\nu \;=\; 4\pi A^2(E+3p+(E+p)U_iU^i) + A^2K_{ij}K^{ij} - \overline{\nabla}_i\nu\,\overline{\nabla}^i(\nu+\beta) \tag{17}$$

$$\underline{\Delta}\,N^i + \frac{1}{3}\overline{\nabla}^i\overline{\nabla}_jN^j \;=\; -16\pi NA^2(E+p)U^i + NB^{-2}K^{ij}\overline{\nabla}_j(6\beta-\nu) \tag{18}$$

$$\Delta_2\left[(NB-1)\,r\sin\theta\right] \;=\; 16\pi NA^2Bp\,r\sin\theta \tag{19}$$

$$\Delta_2\,\zeta \;=\; 8\pi A^2\left[p+(E+p)U_iU^i\right] + \frac{3}{2}A^2K_{ij}K^{ij} - \overline{\nabla}_i\nu\overline{\nabla}^i\nu\ , \tag{20}$$

where the following notations have been introduced [see also Eq. (11)]

$$\zeta := \ln(AN)\ , \quad \beta := \ln B\ , \tag{21}$$

and $\overline{\nabla}_i$ denotes the covariant derivative with respect to the flat 3-metric $f_{ij} = \mathrm{diag}(1, r^2, r^2\sin^2\theta)$, $\underline{\Delta} = \overline{\nabla}_i\overline{\nabla}^i$ the corresponding Laplacian and Δ_2 is the Laplacian in the 2-dimensional space spanned by (r,θ):

$$\Delta_2 := \frac{\partial^2}{\partial r^2} + \frac{1}{r}\frac{\partial}{\partial r} + \frac{1}{r^2}\frac{\partial^2}{\partial\theta^2}\ . \tag{22}$$

In Eqs. (17)-(20), U^i denotes the spatial components of the fluid 3-velocity $\mathbf{U}$ [cf. Eq. (7)]. They can be expressed as

$$U^r = -\frac{N^r}{N}, \quad U^\theta = -\frac{N^\theta}{N}, \quad U^\varphi = \frac{1}{N}(\Omega - N^\varphi), \tag{23}$$

and Γ is deduced from $\mathbf{U}$ by means of Eq. (8):

$$\Gamma = \left(1 - A^2[(U^r)^2 + r^2(U^\theta)^2] - B^2r^2\sin^2\theta(U^\varphi)^2\right)^{-1/2}\ . \tag{24}$$

We have also introduced the energy density E as measured by the Eulerian observer:

$$E = \mathbf{n}\cdot\mathbf{T}\cdot\mathbf{n} = \Gamma^2(e+p) - p\ . \tag{25}$$

Another quantity not yet defined and which appears in Eqs. (17)-(20) is the extrinsic curvature tensor $\mathbf{K}$ of the hypersurface Σ_t.

D. Equation of state

The above equations must be supplemented by an equation of state (EOS), i.e. a relation between H, which appears in the first integral (10), and e and p which appear in the source terms of the Einstein equations (17)-(20), via Eq. (25). For the incompressible matter we are considering, we choose this EOS to be

$$e(H) \;=\; \rho_0 \tag{26}$$

$$p(H) \;=\; \rho_0(\exp(H)-1) \tag{27}$$

$$n(H) \;=\; \rho_0/m_{\rm B}\ , \tag{28}$$

where ρ_0 is a constant, representing the constant proper energy density of the fluid.

III. NUMERICAL CODE AND ITS TESTS

A. Numerical technique

The basic idea is to solve the equations presented in Sec. II by means of an iterative scheme to get an axisymmetric stationary solution, and then to introduce some triaxial perturbation and resume the iterative scheme. If the perturbation is damped (resp. grows) as long as the iteration proceeds, the equilibrium configuration will be declared stable (resp. unstable). This procedure has been used already in the works [12, 13]. We shall prove here, by comparison with the analytical result, that it correctly locates the secular instability point along the Maclaurin sequence.

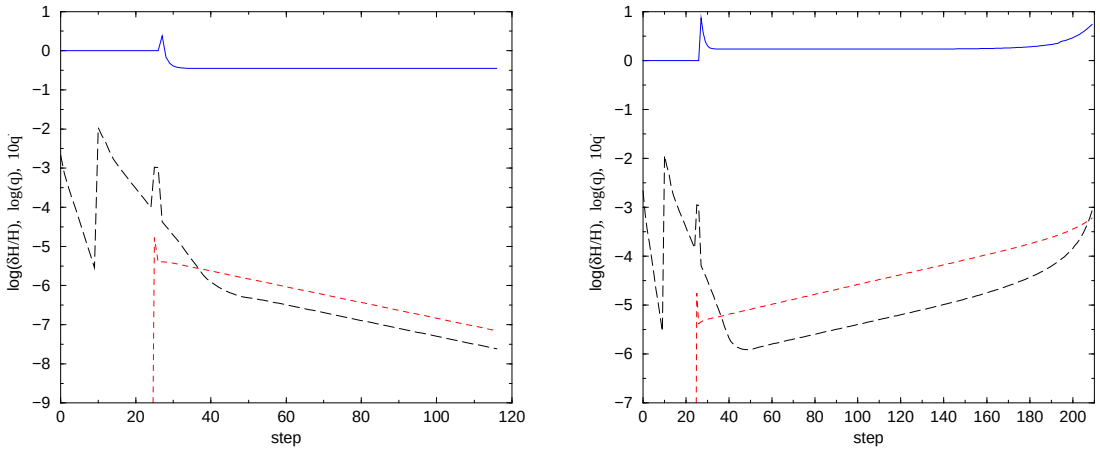

FIG. 1: Evolution during the iterative procedure of the convergence indicator $\delta H/H$ (long-dashed line), the triaxial perturbation q (short-dashed line) and its growth rate $\dot{q}$ (solid line). The left figure corresponds to a stable configuration with respect to nonaxisymmetric perturbation, the right one an unstable one. $\delta H/H$ and q are depicted in logarithmic units, while $\dot{q}$ is multiplied by 10 for better readability. The discontinuity at step 10 is due to the switch of the rotation and that at step 25 to the switch of the triaxial perturbation.

We solve the system of non-linear elliptic equations (17)-(20) by means of the multi-domain spectral method presented in Ref. [31]. The nice feature of this method is that it introduces surface-fitted coordinates (ξ, θ', φ'), so that the density discontinuity at the stellar surface is exactly located at the boundary between two domains. In this way, all the fields are C^∞ functions in each domain. This avoids any spurious oscillations (Gibbs phenomenon) and results in a very high precision. As discussed in Sec. I C, this technique constitutes the major improvement with respect to the numerical method used in Ref. [13]. Another difference with Ref. [13] is that we employ the technique presented in Ref. [32] to solve the vector elliptic equation (18) for the shift vector. In particular, we solve for the Cartesian components of the shift vector, whereas [13] solved for the spherical components.

A weak point of the surface-fitted coordinate technique of Ref. [31] is that the transformation from the computational coordinates (ξ, θ', φ') to the physical ones (r, θ, φ) becomes singular when the ratio of polar to equatorial radius $r_{\rm p}/r_{\rm eq}$ is lower than $\sim 1/3$. This prevents us from computing very flattened configurations, but fortunately this causes no trouble in reaching the Maclaurin-Jacobi bifurcation point, which is at $r_{\rm p}/r_{\rm eq} \simeq 0.58$.

The iterative procedure is as follows. First one must set a value of the central enthalpy H_c and the rotation frequency Ω, in order to pick out a unique rotating axisymmetric configuration. The iteration is then started from very crude values: flat spacetime and spherical stellar shape. We solve the Einstein equations (17)-(20) with the spherical energy density and pressure distribution in their right-hand side. We then plug the obtained value of ν in the first integral of motion (10), along with H_c, to get the enthalpy field H. The zero of this field defines the new stellar surface to which we adapt the computational coordinates (ξ, θ', φ') (see [31] for details). From H we compute new values of the energy density and pressure according to the EOS (26)-(27). These values are then put on the right-hand side of the Einstein equations (17)-(20) and a new iteration begins. Usually the rotation velocity is set to zero for the ten first steps. It is then switched on, either integrally or (for very rapidly rotating configurations) gradually. The convergence of the procedure is monitored by computing the relative difference $\delta H/H$ between the enthalpy fields at two successive steps (long-dashed line in Fig. 1). The iterative procedure is stopped when $\delta H/H$ goes below a certain threshold, typically 10^{-7}, or for high precision computations 10^{-12}.

After this convergence has been achieved, we switch on a triaxial $m = 2$ perturbation by modifying the metric potential ν according to

$$\nu \to \nu \left(1 + \varepsilon \sin^2\theta \cos 2\varphi\right) \ , \tag{29}$$

where ε is a small constant, typically $\varepsilon \simeq 10^{-5}$ to 10^{-3}. Then we continue the iteration procedure as described above, without any further modification of the equations. At each step, we evaluate the quantity

$$q := \max \sqrt{\hat{\nu}_2^2 + \hat{\nu}_3^2} \ , \tag{30}$$

where $\hat{\nu}_2$ and $\hat{\nu}_3$ are the $m = 2$ coefficients of the Fourier expansion of the φ part of ν:

$$\nu(\varphi) = \hat{\nu}_0 + \hat{\nu}_2 \cos(2\varphi) + \hat{\nu}_3 \sin(2\varphi) + \hat{\nu}_4 \cos(4\varphi) + \hat{\nu}_5 \sin(4\varphi) + \cdots \tag{31}$$

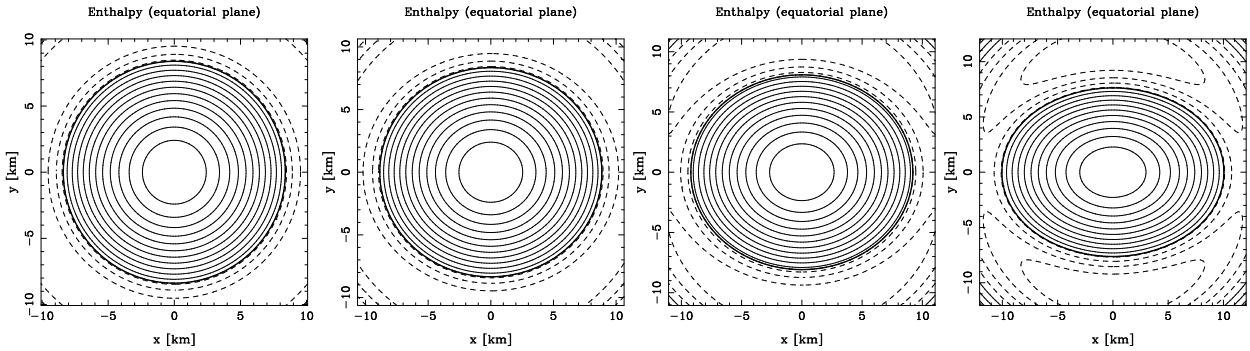

FIG. 2: Isocontours of the enthalpy H in the equatorial plane at steps 20, 150, 180 and 200 for the unstable model presented in Fig. 1. Dashed lines denote negative values of H, which correspond to the exterior of the star. The thick solid line denotes the stellar surface.

and the max in Eq. (30) is taken over all the r and θ coefficients. q is used to monitor the evolution of the triaxial perturbation: if $q \to 0$ as the iteration proceeds, we conclude that the perturbation decays and the axisymmetric configuration is a stable one. In the vicinity of the marginally stable configuration, the decay or growth of the perturbation turns out to be pretty small. In order to facilitate the diagnostic, we monitor instead the *relative* growth rate of the $m = 2$ part, defined as

$$\dot{q} := \frac{q - q_{\text{previous step}}}{q_{\text{previous step}}} \, . \tag{32}$$

After some transitory regime, $\dot{q}$ turned out to be constant. If $\dot{q} > 0$ (resp. $\dot{q} < 0$) we conclude that the configuration is unstable (resp. stable). The behaviors of $\delta H/H$, q and $\dot{q}$ in two typical computations are shown in Fig. 1, whereas Fig. 2 depicts the development of the triaxial instability.

Note that the above method does not require to specify some value of viscosity. Whatever this value, the effect of viscosity is simulated by the rigid rotation profile that we impose at each step in the iterative procedure via Eq. (23). If we consider the iteration as mimicking some time evolution, this means that the time elapsed between two successive steps has been long enough for the actual viscosity to have rigidified the fluid flow. Consequently, a quantity that we cannot get by our method is the instability time scale. As recalled in the Introduction, this time scale depends upon the actual value of viscosity, but not the instability itself.

The numerical code implementing the above procedure has been constructed upon the C++ library Lorene [33]. Numerical computations have been performed on SGI Origin200 as well as Linux PC workstations. Three domains have been used, the innermost one corresponding to the interior of the star, and the outermost one extending to spacelike infinity by means of a suitable compactification (see [31] for details). The number of spectral coefficients used in each domain is $N_r \times N_\theta \times N_\varphi = 33 \times 17 \times 4$. The corresponding memory requirement is 40 MB and a typical CPU time (e.g. corresponding to the first 60 steps of Fig. 1, which are sufficient to conclude about the stability of the configuration) is 3 min on an Intel Pentium IV 1.5 GHz processor.

B. Test of the numerical code

Numerous tests have been performed to assess the validity of the method and the accuracy of the numerical code. We present here successively tests for axisymmetric configurations in general relativity and tests about the determination of the triaxial instability point in the Newtonian limit. Tests regarding the triaxial instability in the relativistic case are deferred to Sec. IV B, where we present a detailed comparison with analytical (post-Newtonian) results.

1. Tests in the axisymmetric regime

The multi-domain spectral technique with surface-fitted coordinates has already been tested in the Newtonian regime, giving a rapidly rotating Maclaurin ellipsoid with a relative error of the order of 10^{-12} [31]. It has been also shown in Ref. [31] that the error is evanescent, i.e. that it decays exponentially with the number of spectral coefficients, which is typical of spectral methods.

TABLE I: Comparison with the numerical results of Ansorg et al. [38] for a highly relativistic stationary axisymmetric model $p_c/\rho_0 = 1$ ($H_c = \ln 2$) and $r_p/r_{eq} = 0.7$, with compaction parameter $M/R_{circ} \sim 0.39$. Meaning of the symbols [in geometrized units ($G = c = 1$)] are as follows: dimensionless angular velocity $\overline{\Omega} := \Omega/\rho_0^{1/2}$, gravitational mass $\overline{M} := M\rho_0^{1/2}$, baryon mass $\overline{M}_B := M_B\rho_0^{1/2}$, circumferential equatorial radius $\overline{R}_{circ} := R_{circ}\rho_0^{1/2}$, angular momentum $\overline{J} := J\rho_0$. Z_p, Z_{eq}^f, and Z_{eq}^b are the redshifts in the polar direction, in the equatorial plane along the direction of motion and opposite to that direction respectively.

	our value	relative diff.
$\overline{\Omega}$	1.4116964	0.0009 %
$\overline{M}$	0.1358182	0.015 %
$\overline{M}_0$	0.1863648	0.014 %
$\overline{R}_{circ}$	0.34548954	0.0039 %
$\overline{J}$	0.01405836	0.0017 %
Z_p	1.7073708	0.001 %
Z_{eq}^f	−0.1625613	0.017 %
Z_{eq}^b	11.3539974	0.00073 %

The accuracy of the computed relativistic axisymmetric models is estimated using two general relativistic virial identities GRV2 [34, 35] and GRV3 [36]. These two virial error indicators are integral identities which must be satisfied by any solution of the Einstein equations and which are not imposed during the numerical procedure (see Ref. [37] for the computation of GRV2 and GRV3). GRV3 is a generalization to general relativity of the classical virial theorem. We have obtained values of GRV2 and GRV3 of the order of 10^{-12} in Newtonian regime and $10^{-8} - 10^{-4}$ for high rotation and high compaction parameter. The virial errors are at least one order of magnitude better than obtained in the previous code used for calculating rapidly rotating strange stars [39, 40, 41, 42, 43, 44, 45, 46].

Another test in the strongly relativistic regime is the comparison with the highly accurate recent code of Ansorg et al. [38], also based on spectral methods but using very different coordinates and resolution scheme. The relative differences defined as diff = |(AKM − GG)/AKM| (where AKM and GG are the values obtained by Ansorg et al. [38] – their Table 1 – and us respectively), are presented in Table I for an incompressible rapidly rotating body with a compaction parameter $M/R_{circ} = 0.393$, where R_{circ} is the circumferential radius of the star. Note that this model is much more relativistic than any realistic neutron star, so that we are really testing the strong field behavior of our code. Table I shows that the agreement with Ansorg et al. is very good, of the order of 10^{-4} or better. For this model, the GRV2 and GRV3 errors from our code are $2\,10^{-5}$ and $3\,10^{-6}$ respectively.

2. Tests about the code capability to find the triaxial instability

Widely used indicators for the onset of instability are the eccentricity e and the ratio of the kinetic energy to the absolute value of the gravitational potential energy $T/|W|$, defined respectively as

$$e^2 = 1 - (r_p/r_{eq})^2 , \tag{33}$$

$$T/|W| = \frac{\Omega J/2}{\Omega J/2 + M_B - M} , \tag{34}$$

where r_p and r_{eq} are the polar and equatorial coordinate radius, J the total angular momentum and M_B the baryon mass. Note that $T/|W|$ is gauge invariant for uniformly rotating incompressible objects[3], while eccentricity is coordinate dependent. In the Newtonian regime, we have employ the code to locate the bifurcation point between the Maclaurin sequence and the Jacobi one, and found it to be at

$$(T/|W|)_{crit} = 0.137526 \quad \text{and} \quad e_{crit} = 0.812667 . \tag{35}$$

Both quantities differ from the exact value $(T/|W|)_{crit,Newt}$ and $e_{crit,Newt}$ [1] by only 10^{-6}.

[3] For compressible bodies, $T/|W|$ can be defined according to Eqs. (20)-(22) of Ref. [47], for which M_B at the denominator of Eq. (34) must be replaced by some "proper" internal energy M_p; in general relativity this last quantity has less physical meaning than the total baryon mass M_B.

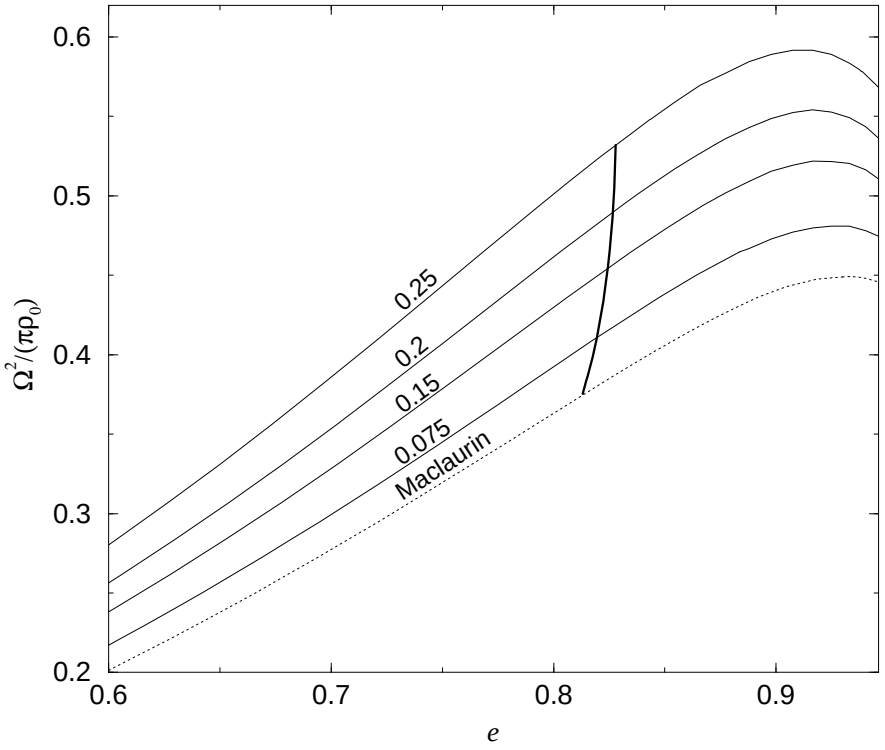

FIG. 3: Square of the angular velocity (in units of $\pi G\rho_0$) as a function of the eccentricity [defined by Eq. (33)] for axisymmetric equilibrium sequences of constant rest mass. Each sequence is labeled by the compaction parameter $M_{\rm s}/R_{\rm s}$ of its nonrotating member. The dotted line denotes the Maclaurin sequence ($M_{\rm s}/R_{\rm s} = 0$). The thick line connects the secular instability points.

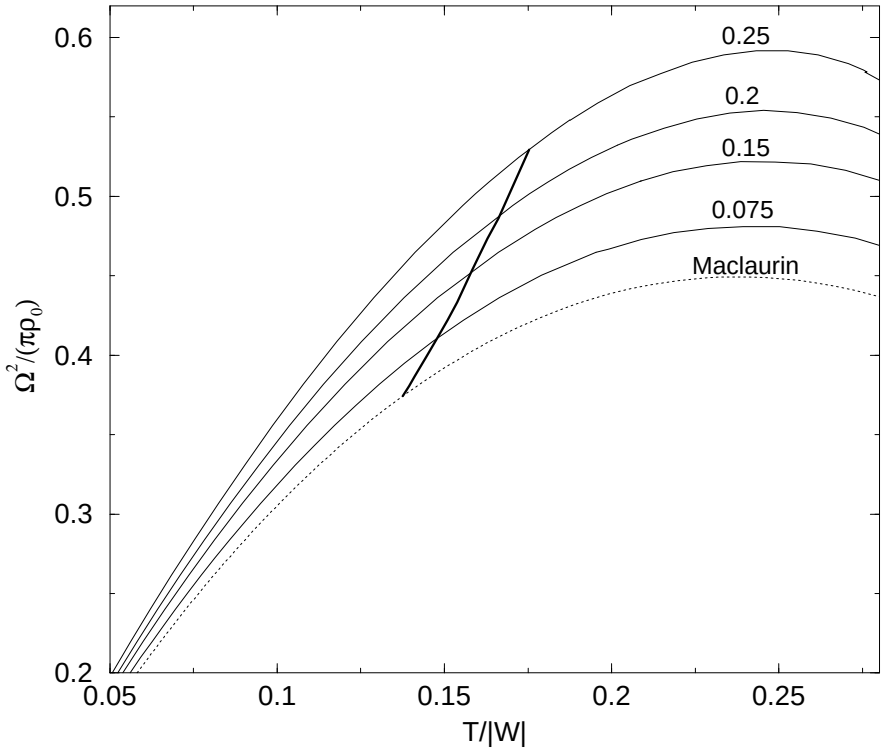

FIG. 4: Square of the angular velocity versus the ratio of the kinetic energy to the absolute value of the gravitational potential energy [defined by Eq. (34)] for the same sequences as in Fig. 3. The thick line connects the secular instability points.

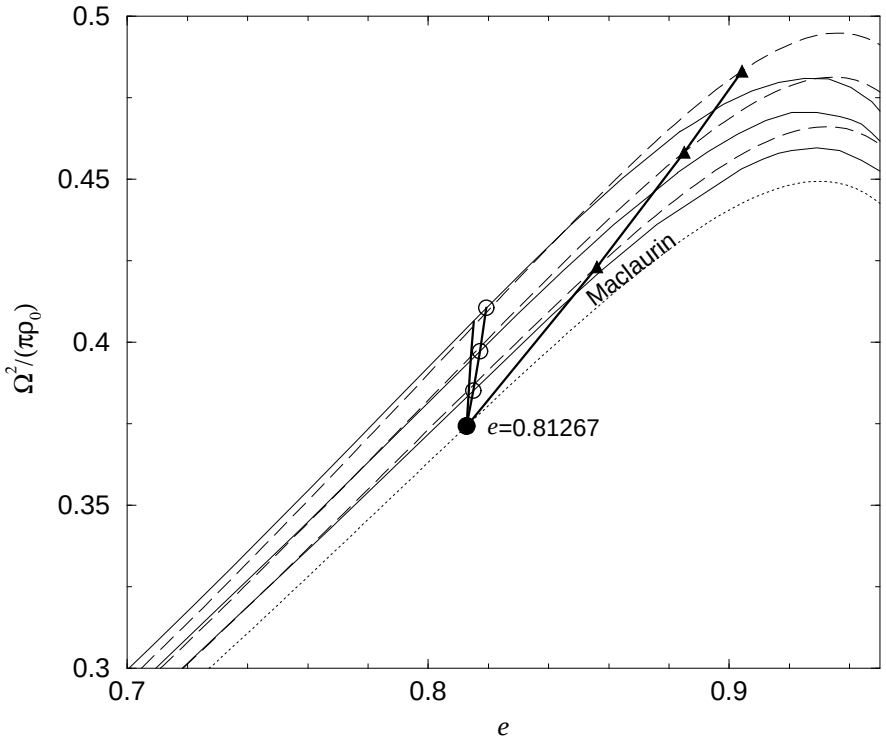

FIG. 5: Comparison between the present relativistic computations of the bar mode instability points (thick solid line with circles) and that of two different PN calculations performed by [10] (thick solid line with triangles) and by [11] (thick solid line). The Newtonian Maclaurin-Jacobi bifurcation point is shown as a filled circle. Thin solid lines and long-dashed lines corresponds respectively to fully relativistic calculations and to the ellipsoidal PN ones of [10] for axisymmetric equilibrium sequences with compaction parameter $M_{\rm s}/R_{\rm s} = 0.075$; 0.05; 0.025 from top to bottom. The dotted line represents the Newtonian Maclaurin sequence ($M_{\rm s}/R_{\rm s} = 0$).

IV. CALCULATIONS AND RESULTS

A. Rotating axisymmetric equilibrium configurations

We present in this section our results about the relativistic analogs of the axisymmetric Newtonian Maclaurin ellipsoids. As mentioned in Sec. III A, the multi-domain spectral technique with surface-fitted coordinates that we employ has some trouble when $r_{\rm p}/r_{\rm eq} < 1/3$. To compute very rapidly rotating configurations, well beyond the Jacobi-like bar mode instability (which is located at $r_{\rm p}/r_{\rm eq} \simeq 0.58$ in the Newtonian regime), we employ a second numerical code for axisymmetric stationary relativistic stars, namely that of Stergioulas [48] (see [49] for a description). More precisely, the multi-domain spectral code has been used for calculating rotating stars with the eccentricity e (or $T/|W|$) lower than $0.92 - 0.87$ (0.23-0.2) for compaction parameters ranging from 0 to 0.25, while Stergioulas' code has been used for higher values. In the overlapping region around $e \sim 0.9$, models computed by both codes agree very well in all computed properties.

We have constructed constant baryon mass sequences of uniformly rotating axisymmetric homogeneous fluid bodies. Each of the sequences is parametrized by the compaction parameter $M_{\rm s}/R_{\rm s}$, where $M_{\rm s}$ and $R_{\rm s}$ are the gravitational mass and circumferential radius of the spherical (non-rotating) member of the sequence. To show the role of relativistic effects we plot in Fig. 3 and Fig. 4 the square of the angular velocity as a function of the eccentricity e and $T/|W|$ respectively for several axisymmetric equilibrium sequences (thin lines) with compaction parameters $M_{\rm s}/R_{\rm s}$ ranging from 0 (Newtonian Maclaurin sequence) to 0.25. We find that in general relativity the rotational velocity along the equilibrium sequence is not much different from that one derived in the Newtonian limit, although a star of a given eccentricity has a little bit higher value of the square of the angular velocity (the biggest difference is near the maximum, and for $M_{\rm s}/R_{\rm s} = 0.25$, it is by 35% higher than the Newtonian one). The location of the maximum of $\Omega^2/(\pi\rho_0)$ weakly depends on the compaction parameter and is only a slightly shifted to lower values of eccentricity and higher values of $T/|W|$ for highly relativistic stars.

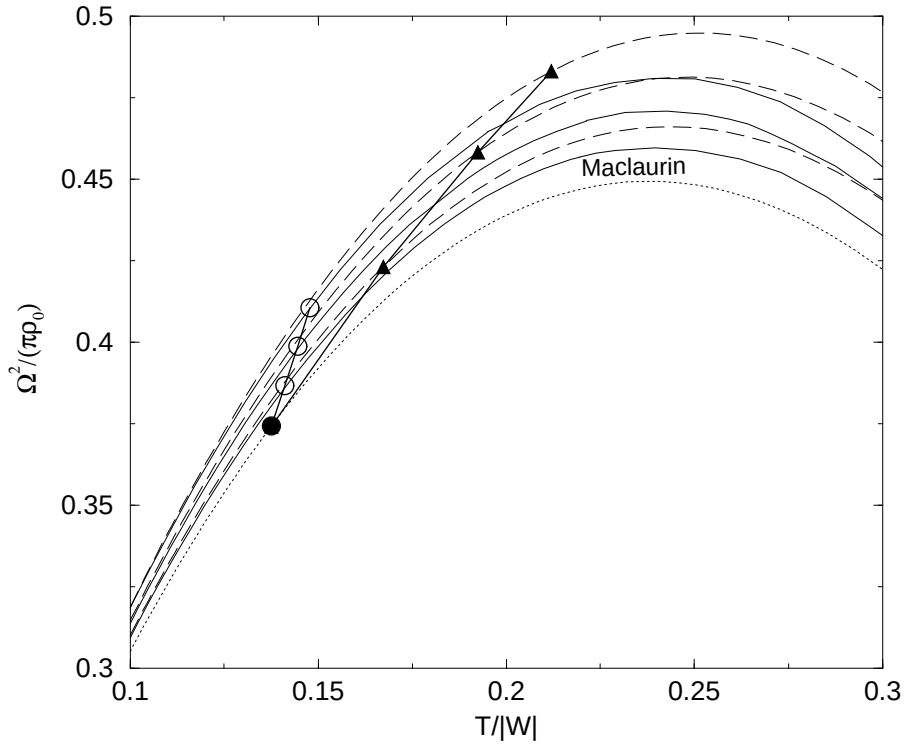

FIG. 6: Square of the angular velocity as a function of the ratio of the kinetic energy to the absolute value of the gravitational potential energy for the same equilibrium sequences as in Fig. 5 (all symbols and lines have the same meaning as in Fig. 5). The thick lines with circles and filled triangles correspond to the secular instability points obtained by us and by [10] respectively.

In Figs. 5 and 6 we compare our fully relativistic sequences with PN equilibrium sequences in the ellipsoidal approximation [10], for compaction parameters $M_{\rm s}/R_{\rm s} = 0.025$, 0.05 and 0.075. Let us recall that, contrary to the Newtonian case, in general relativity the figure of equilibrium of rotating incompressible bodies is not an ellipsoid (with respect to the employed coordinates). However as it can be seen for low compactness the ellipsoidal PN models and fully relativistic models are in close agreement up to the value of eccentricity ~ 0.9 and $T/|W| \sim 0.2$. The discrepancy increases as eccentricity increases. For $M_{\rm s}/R_{\rm s} = 0.075$ and $e = 0.9$ the value of $\Omega^2/(\pi\rho_0)$ is overestimated by 3% using the ellipsoidal approximation.

For high compaction parameter ($M_{\rm s}/R_{\rm s} > 0.1$) comparison between our fully relativistic calculations (Figs. 3 and 4) and PN ones (Fig. 3 in [10]) shows that the ellipsoidal approximation does not provide a good description of equilibrium axisymmetric configurations. We find a more pronounced increase of the angular velocity with compactness at any given value of eccentricity. The relative differences are 10% and 20% for $M_{\rm s}/R_{\rm s} = 0.15$ and 0.25 respectively and $e < 0.8$ (there are much larger for higher value of e). Moreover according to [10] the location of the maximum of $\Omega^2/(\pi\rho_0)$ is shifted to higher values of e with respect to Newtonian one, while we find the opposite tendency, in agreement with [11].

B. Secular bar mode instability

1. *Our results*

Some important quantities at the viscosity driven instability points for different values of compaction parameter are reported in Table II. We are using two kinds of compaction parameters: $M_{\rm s}/R_{\rm s}$ already defined and the *proper compaction parameter* $M/R_{\rm circ}$, where $R_{\rm circ}$ is the circumferential radius, i.e. the length of the equator (as given by the metric) divided by 2π of the actual configuration (unlike $R_{\rm s}$ which is the circumferential radius of the non rotating star having the same baryon mass).

Our results are shown as thick lines in Figs. 3, 4 and 7. According to our analysis the critical value of the eccentricity very weakly depends on the compaction parameter and for $M_{\rm s}/R_{\rm s} = 0.275$ is by only 2% larger than Newtonian value

TABLE II: **Jacobi-like instability points along relativistic sequences.** The symbols are as follows (all values are for axisymmetric configurations at the instability point): H_c is the central enthalpy; $\frac{M}{R_{\rm circ}}$ is the proper compaction parameter, where $R_{\rm circ}$ is circumferential radius; $\frac{M_{\rm s}}{R_{\rm s}}$ is the compaction parameter of nonrotating spherical configurations with the same rest mass as the marginally stable configuration; N_c is central lapse; $\Omega^2/(\pi\rho_0)$ is a square of the angular velocity in the unit $\pi G\rho_0$; $e_{\rm crit}$ and $({\rm T}/|{\rm W}|)_{\rm crit}$ are eccentricity and the ratio of the kinetic energy to the absolute value of the gravitational potential energy at the instability points; GRV2 and GRV3 are virial errors.

H_c	$\frac{M_{\rm s}}{R_{\rm s}}$	$\frac{M}{R_{\rm circ}}$	N_c	$\Omega^2/(\pi\rho_0)$	$e_{\rm crit}$	$({\rm T}/\|{\rm W}\|)_{\rm crit}$	GRV2	GRV3
—	0	0	1	0.37423	0.81267	0.13753	—-	3.e-12
0.01	0.025	0.0227	0.95976	0.38670	0.81528	0.14119	-3e-07	-5.e-05
0.02	0.050	0.0438	0.92172	0.39885	0.81750	0.14464	2e-06	5e-05
0.04	0.094	0.0815	0.85174	0.42222	0.82096	0.15097	-3e-07	6e-05
0.05	0.113	0.0984	0.81955	0.43346	0.82231	0.15389	-4e-06	-2e-05
0.07	0.151	0.1289	0.76022	0.45512	0.82439	0.15930	8e-07	9e-05
0.09	0.181	0.1556	0.70691	0.47570	0.82584	0.16422	-2e-05	-5e-05
0.11	0.205	0.1792	0.65885	0.49528	0.82684	0.16871	9e-06	2e-05
0.12	0.219	0.1899	0.63658	0.50474	0.82721	0.17083	-1e-06	-7e-05
0.13	0.230	0.2000	0.61537	0.51403	0.82755	0.17290	-1e-05	-1e-4
0.15	0.250	0.2187	0.57593	0.53192	0.82795	0.17674	2e-05	3e-05
0.16	0.258	0.2272	0.55757	0.54057	0.82809	0.17859	1e-05	-6e-05
0.18	0.275	0.2430	0.52322	0.55748	0.82838	0.18220	-3e-05	-2e-4

of the onset of the secular bar mode instability. The critical value of the ratio of the kinetic energy to the absolute value of the gravitational potential energy $(T/|W|)_{\rm crit}$ for compaction parameter as high as 0.275 is by 30% (Table II) higher than the Newtonian value. The dependence of $(T/|W|)_{\rm crit}$ on the compactness can be very well approximated by the function

$$(T/|W|)_{\rm crit} \simeq (T/|W|)_{\rm crit,Newt} + \begin{cases} 0.148\,x(x+1) & \text{for} \quad x := M/R_{\rm circ} \\ 0.126\,x(x+1) & \text{for} \quad x := M_{\rm s}/R_{\rm s} \end{cases} \tag{36}$$

2. Comparison with PN calculations

The comparison between our relativistic calculations of the viscosity driven instability and the corresponding two different PN calculations derived by [10] and by [11] is shown in Fig 5, 6 and 8. Shapiro and Zane [10] employ an energy variational principle to determine equilibrium shape and stability of homogeneous triaxial ellipsoids. The method used by them is valid for arbitrary rotation rate, but only for constant density bodies. Di Girolamo and Vietri [11] determined the value of the eccentricity and $\Omega^2/(\pi\rho_0)$ at the instability onset point using Landau's theory of second-order phase transitions. This method is the extension to PN regime of that used by Bertin and Radicati [3] for the Newtonian treatment of bar mode instability and valid for any equation of state. Considering the dependence of $\Omega^2/(\pi\rho_0)$ with respect to the eccentricity (Fig. 5) we found good agreement between our results and the PN ones of [11]. As can be seen, both calculations show much weaker influence of relativistic effects on location of the instability onset point than Shapiro & Zane PN calculations.

Figure 8 shows the dependence of the critical eccentricity and the critical value of $T/|W|$ on the compaction parameter $M_{\rm s}/R_{\rm s}$. The Authors of [11] use a proper "conformal compaction parameter" $M_{\rm c}/R_{\rm c} := 4\pi\rho_0/3R_{\rm c}^2$, where $R_{\rm c} = (a_1a_2a_3)^{1/3}$, a_1, a_2, a_3 being the ellipsoid semiaxes. In order to make a comparison between our relativistic calculations and those of [11] we find the $M_{\rm s}/R_{\rm s}$ corresponding to their $M_{\rm c}/R_{\rm c}$ using the formula $M_{\rm c}/R_{\rm c} = 0.25M_{\rm s}/R_{\rm s}(1 - M_{\rm s}/R_{\rm s} + (1 - 2M_{\rm s}/R_{\rm s}))^2$ (see [50], expression [4], p. 422). This formula is valid in the spherical limit, but the difference between the proper "conformal compaction parameter" and the "spherical conformal compaction parameter" is at most 3 %.

According to our analysis the critical value of the eccentricity depends very weakly on the compaction parameter (solid line); this is in agreement with the PN calculations by Di Girolamo & Vietri [11]. The relative differences between our and their PN calculations are less than 1%. A much stronger weakening of the bar mode instability by general relativity is suggested by the PN study of Shapiro & Zane [10], who find that $e_{\rm crit}$ (dashed line in the left panel of Fig. 8) could be as large as 0.94 at $M_{\rm s}/R_{\rm s} = 0.25$. This discrepancy may be ascribed mainly to the ellipsoidal

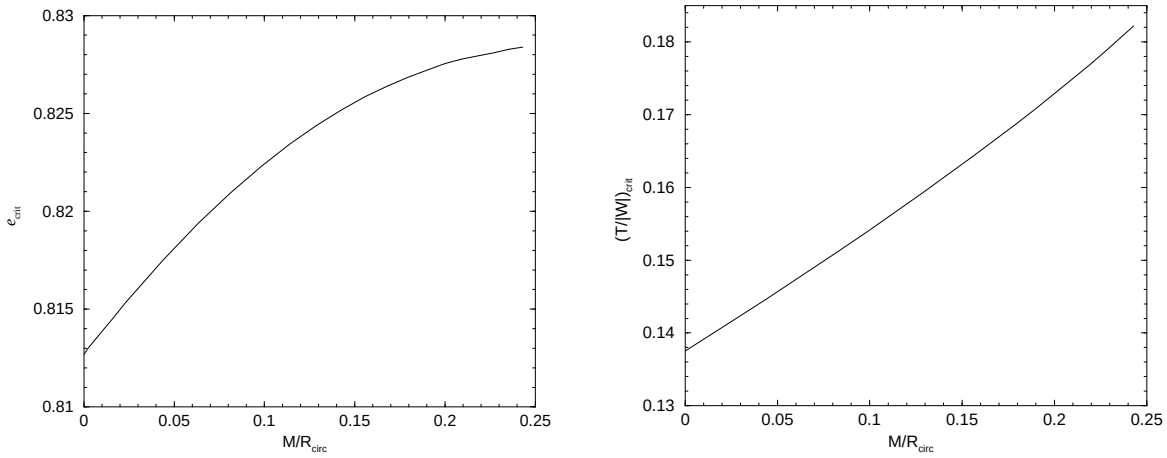

FIG. 7: Eccentricity (left) and ratio of the kinetic energy to the absolute value of the gravitational potential energy (right) at the onset of the secular bar mode instability, versus the compaction parameter $M/R_{\rm circ}$.

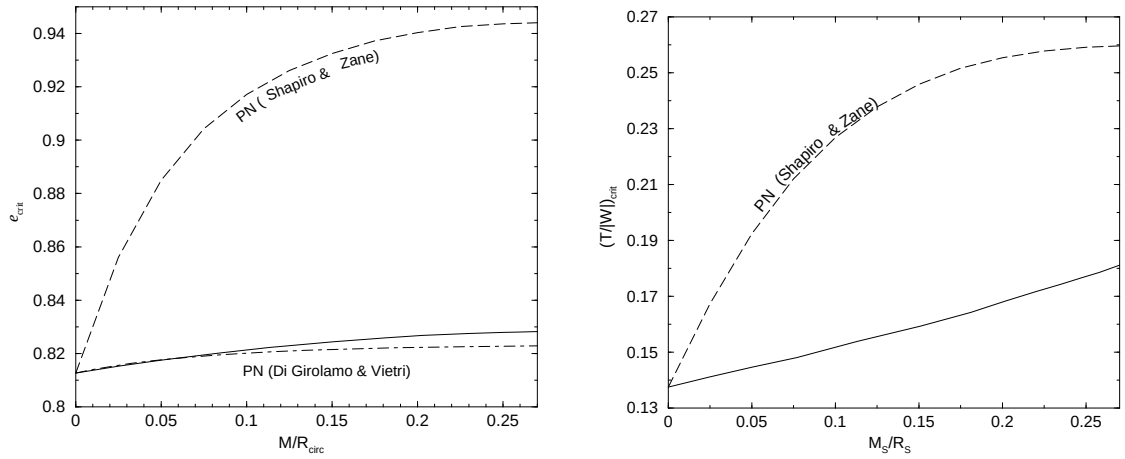

FIG. 8: Eccentricity (left) and ratio of the kinetic energy to the absolute value of the gravitational potential energy (right) at the onset of the secular bar mode instability, versus the compaction parameter $M_{\rm s}/R_{\rm s}$. Our results are denoted by the solid line. The dashed line and the dash-dotted line correspond to the PN calculations by [10] and [11] respectively.

approximation for the deformation and equilibrium shape. We refer to the article [11] for a detailed explanation of discrepancies between the two PN calculations of instability points.

The right panel of Fig. 8 presents the comparison between [10] and our calculation of the critical $T/|W|$ as a function of the compaction parameter $M_{\rm s}/R_{\rm s}$. We found that for the compaction parameter as high as 0.05; 0.15; 0.25 $(T/|W|)_{\rm crit}$ is only by 5%; 16%; 28% higher than Newtonian value, while according to Ref. [10], the increase is 40%; 79%; 88% respectively.

According to our study relativistic effects weaken the Jacobi-like bar mode instability (solid line in Figs. 3, 4, 7 and 8), but the stabilizing effect is not very strong. This is in agreement with the PN calculations [11].

V. SUMMARY

Triaxial instabilities of rotating compact stars can play an important role as emission mechanisms of gravitational waves in the frequency range of the forthcoming interferometric detectors. A rapidly rotating neutron star can spontaneously break its axial symmetry if the ratio of the rotational kinetic energy to the absolute value of the gravitational potential energy $T/|W|$ exceeds some critical value. We have investigated the effects of general relativity upon the nonaxisymmetric viscosity-driven bar mode instability of incompressible, uniformly rotating stars. This is the relativistic analog of the Newtonian Maclaurin-Jacobi bifurcation point.

Our method of finding the instability point is similar to that used in Ref. [13] for compressible fluid stars. The main improvement with respect to this work regards the numerical technique. We have indeed introduced surface-fitted coordinates, which enable us to treat the strongly discontinuous density profile at the surface of incompressible bodies. This avoids any Gibbs-like phenomenon and results in a very high precision, as demonstrated by comparison with the analytical result for the Newtonian Maclaurin-Jacobi bifurcation point, that our code has retrieved with a relative error of 10^{-6}.

According to our results, general relativity weaken the Jacobi-like bar mode instability: the values of T/W, eccentricity and $\Omega^2/(\pi\rho_0)$ increase at the onset of instability above the Newtonian values. This general tendency is in agreement with PN analytical results [10, 11] for rigidly rotating incompressible bodies and with the numerical calculations of [13] for relativistic polytropes. However we found that the stabilizing effect of general relativity is much weaker than that obtained in the PN treatment of [10]. The critical value of the ratio of the kinetic energy to the absolute value of the gravitational potential energy $(T/|W|)_{\rm crit}$ for a compaction parameter as high as 0.275 is only 30% larger than the Newtonian value, whereas it has been found 90% larger by [10].

According to our analysis the critical value of the eccentricity very weakly depends on the compaction parameter and for a compaction parameter as high as 0.275 is only 2% (16% according to [10]) larger than the Newtonian value of the onset of the secular bar mode instability. Regarding the dependence of $\Omega^2/(\pi\rho_0)(e_{\rm crit})$ and $e_{\rm crit}$ with respect to compactness, we found very good agreement between our result and the recent PN ones of [11], the relative differences being lower than 1%.

Acknowledgments

We are grateful to Nick Stergioulas and Tristano Di Girolamo for helpful discussions and to Brandon Carter for reading the manuscript. We also thank Stuart Shapiro and Silvia Zane for providing tables of their results and Tristano Di Girolamo and Mario Vietri for providing their results prior to publication. This work has been funded by the following grants: KBN grants 5P03D01721; the Greek-Polish Joint Research and Technology Program EPAN-M.43/2013555 and the EU Program "Improving the Human Research Potential and the Socio-Economic Knowledge Base" (Research Training Network Contract HPRN-CT-2000-00137).

[1] S. Chandrasekhar, *Ellipsoidal figures of equilibrium* (Yale University Press, New Haven, 1969).
[2] W.H. Press and S.A. Teukolsky, Astrophys. J. **181**, 513 (1973).
[3] G. Bertin and L.A. Radicati, Astrophys. J. **206**, 815 (1976).
[4] D.M. Christodoulou, D. Kazanas, I. Shlosman, and J.E. Tohline, Astrophys. J. **446**, 472 (1995).
[5] N. Andersson, *Gravitational waves from instabilities in relativistic stars*, to appear in Class. Quantum Grav.
[6] J.R. Ipser and R.A.Managan, Astrophys. J. **250**, 352 (1981).
[7] S. Chandrasekhar, Astrophys. J. **148**, 621 (1967).
[8] S. Chandrasekhar, Astrophys. J. **167**, 455 (1971).
[9] K. Taniguchi, *Ellipsoidal figures of equilibrium in the first post-Newtonian approximation of general relativity*, PhD Thesis, Kyoto University (1999), Chap. 7.
[10] S.L. Shapiro and S. Zane, Astrophys. J. Suppl. Ser. **117**, 531 (1998).
[11] T. Di Girolamo and M. Vietri, *Post-Newtonian treatment of bar mode instability in rigidly rotating equilibrium configurations for neutron stars*, in preparation (2002).
[12] S. Bonazzola, J. Frieben, and E. Gourgoulhon, Astrophys. J. **460**, 379 (1996).
[13] S. Bonazzola, J. Frieben, and E. Gourgoulhon, Astron. Astrophys. **331**, 280 (1998).
[14] R.A. James, Astrophys. J. **140**, 552 (1964).
[15] D. Skinner and L. Lindblom, Astrophys. J. **461**, 920 (1996).
[16] N. Stergioulas and J.L. Friedman, Astrophys. J. **492**, 301 (1998).
[17] S.M. Morsink, N. Stergioulas, and S.R. Blatting, Astrophys. J. **510**, 854 (1999).
[18] S. Detweiler, in *Frontiers in Numerical Relativity*, edited by C.R. Evans, L.S. Finn, and D.W. Hobill (Cambridge University Press, Cambridge, 1989), p. 43.
[19] S. Bonazzola, E. Gourgoulhon, and J-A. Marck, Phys. Rev. D **56**, 7740 (1997).
[20] T.W. Baumgarte, G.B. Cook, M.A. Scheel, S.L. Shapiro, and S.A. Teukolsky, Phys. Rev. D **57**, 7299 (1998).
[21] E. Gourgoulhon, P. Grandclément, and S. Bonazzola, Phys. Rev. D **65**, 044020 (2002).
[22] J.L. Friedman, K. Uryu, and M. Shibata, Phys. Rev. D **65**, 064035 (2002).
[23] A. Lichnerowicz, *Relativistic hydrodynamics and magnetohydrodynamics* (Benjamin, New York, 1967).
[24] B. Carter, in *Active Galactic Nuclei*, edited by C. Hazard and S. Mitton (Cambridge University Press, Cambridge, England, 1979), p. 273.
[25] R.H. Boyer, Proc. Cambridge Phil. Soc. **61**, 527 (1965).

[26] S. Bonazzola, E. Gourgoulhon, M. Salgado, and J.-A. Marck, Astron. Astrophys. **278**, 421 (1993).
[27] E. Gourgoulhon, P. Haensel, R. Livine, E. Paluch, S. Bonazzola, and J.-A. Marck, Astron. Astrophys. **349**, 851 (1999).
[28] A. Papapetrou, Ann. Inst. H. Poincaré A **4**, 83 (1966).
[29] W. Kundt and M. Trümper, Z. Physik **192**, 419 (1966).
[30] B. Carter, J. Math. Phys. **10**, 70 (1969).
[31] S. Bonazzola, E. Gourgoulhon, and J-A. Marck, Phys. Rev. D **58**, 104020 (1998).
[32] P. Grandclément, S. Bonazzola, E. Gourgoulhon, and J.-A. Marck, J. Comp. Phys. **170**, 231 (2001).
[33] `http://www.lorene.obspm.fr/`
[34] S. Bonazzola, Astrophys. J. **182**, 335 (1973).
[35] S. Bonazzola and E. Gourgoulhon, Class. Quantum Grav. **11**, 1775 (1994).
[36] E. Gourgoulhon and S. Bonazzola, Class. Quantum Grav. **11**, 443 (1994).
[37] T. Nozawa, N. Stergioulas, E. Gourgoulhon, and Y. Eriguchi, Astron. Astrophys. Suppl. Ser. **132**, 431 (1998).
[38] M. Ansorg, A. Kleinwaechter, and R. Meinel, Astron. Astrophys. **381**, L49 (2002).
[39] E. Gourgoulhon, P. Haensel, R. Livine, E. Paluch, and S. Bonazzola, J.-A. Marck, Astron. Astrophys. **349**, 851 (1999).
[40] D. Gondek-Rosińska, P. Haensel, J. L. Zdunik, and E. Gourgoulhon, ASP Conf. Ser. **202**, 661, astro-ph/0009282 (2000).
[41] J.L. Zdunik, T. Bulik, W. Kluźniak, P. Haensel, and D. Gondek-Rosińska, Astron. Astrophys. **359**, 143 (2000).
[42] J.L. Zdunik, P. Haensel, D. Gondek-Rosińska, and E. Gourgoulhon, Astron. Astrophys. **356**, 612 (2000).
[43] D. Gondek-Rosińska, T. Bulik, L. Zdunik, E. Gourgoulhon, S. Ray, J. Dey, and M. Dey, Astron. Astrophys. **363**, 1005 (2000).
[44] D. Gondek-Rosińska, N. Stergioulas, T. Bulik, W. Kluźniak, and E. Gourgoulhon, Astron. Astrophys. **380**, 190 (2001).
[45] D. Gondek-Rosińska, T. Bulik, W. Kluźniak, L. Zdunik, and E. Gourgoulhon, ESA SP-**459**, 223, astro-ph/0012540 (2001).
[46] P. Amsterdamski, T. Bulik, D. Gondek-Rosińska, and W. Kluźniak, Astron. Astrophys. **381**, L21 (2002).
[47] J.L. Friedman, J.R. Ipser, and L. Parker, Astrophys. J. **304**, 115 (1986).
[48] N. Stergioulas and J.L. Friedman, Astrophys. J. **444**, 30 (1995).
[49] N. Stergioulas, Living Rev. Relativity **1**, 8, `http://www.livingreviews.org/Articles/Volume1/1998-8stergio/` (1998).
[50] A.P. Lightman, W.H. Press, R.H. Price, and S.A. Teukolsky, *Problem Book in Relativity and Gravitation* (Princeton Univ. Press, Princeton, 1979).